Duncan, R.A., Larsen, H.C., Allan, J.F., et al., 1996
Proceedings of the Ocean Drilling Program, Initial Reports, Vol. 163

4. SITE 989[1]

Shipboard Scientific Party[2]

HOLE 989A

Date occupied: 16 September 1995

Date departed: 17 September 1995

Time on hole: 20 hr, 35 min

Position: 63°31.355′N, 39°54.113′W

Bottom felt (drill-pipe measurement from the rig floor, m): 470.4

Distance between rig floor and sea level (m): 10.9

Water depth (drill-pipe measurement from sea level, m): 459.5

Total depth (from rig floor, m): 491.8

Penetration (m): 21.4

Number of cores (including cores having no recovery): 3

Total length of cored section (m): 21.4

Total core recovered (m): 16.0

Core recovery (%): 74.9

Oldest sediment cored:
Depth (mbsf): 3
Nature: rounded cobbles of continentally derived igneous and metamorphic rocks, probably ice rafted
Earliest age: unknown, probably Quaternary

Top of basement:
Depth (mbsf): 3
Nature: massive, moderately vesicular aphyric basalt
Measured velocity (km/s): 4.8–5.3 (5.1 average)

HOLE 989B

Date occupied: 17 September 1995

Date departed: 20 September 1995

Time on hole: 3 days, 3 hr, 30 min

Position: 63°31.355′N, 39°54.110′W

Bottom felt (drill-pipe measurement from the rig floor, m): 470.4

Distance between rig floor and sea level (m): 10.9

Water depth (drill-pipe measurement from sea level, m): 459.5

Total depth (from rig floor, m): 554.6

Penetration (m): 84.2

Number of cores (including cores having no recovery): 14

Total length of cored section (m): 80.2

Total core recovered (m): 74.0

Core recovery (%): 92.9

Oldest sediment cored:
Depth (mbsf): 4
Nature: rounded cobbles of continentally derived igneous and metamorphic rocks, probably ice rafted
Earliest age: unknown, probably Quaternary

Top of basement:
Depth (mbsf): 4
Nature: massive, moderately vesicular aphyric basalt
Measured velocity (km/s): 6.0–6.4

Principal results: Site 989 is located 43 km east of the East Greenland coast, within the southern drilling transect EG63 (Figs. 1, 2), and is one of the three drill sites planned for this transect. Drilling at Leg 152 Sites 915 and 917 had penetrated a thick lava sequence that recorded development from early continental crust-contaminated volcanism, through transitional picritic and tholeiitic volcanism contemporaneous with breakup, into steady-state oceanic volcanism. Site 989 was selected to penetrate and sample the oldest lavas of the seaward-dipping reflector sequence that overlies the breakup unconformity and underlying, layered prerift crust. The primary drilling objectives at this site were to (1) determine the stratigraphy, composition, age, and eruption environment of the volcanic rocks above the breakup unconformity, (2) determine the nature and age of the breakup unconformity, and (3) determine the nature and deformation of the continental basement and/or prerift sediments beneath the volcanic sequence.

Lithologic Unit I is a thin layer (0–4 m below seafloor [mbsf]) of Quaternary(?) glaciomarine sediments unconformably overlying basaltic basement (igneous Units 1 and 2). The only material recovered consists of discrete rock fragments, including gneiss, aphyric basalts and metabasalts, quartzite, and dolerite. The lithologies of these clasts are consistent with an ice-rafted origin, even though no finer grained matrix was recovered. The relatively weak nature of the sediments at Site 989 suggests that these are glaciomarine deposits, rather than overcompacted glacial tills.

Two igneous flow units were recognized in the core recovered from the interval at 4–84 mbsf (Hole 989B). From seismic data, these are interpreted to lie just above the breakup unconformity and stratigraphically below the lavas drilled at Site 917, and thus represent the oldest part of the SDRS. Igneous Unit 1 is at least 69 m thick, the thickest lava flow yet reported from an SDRS. It is notable for its constant grain size, constant vesicularity, high mesostasis content, and repeated bands showing quench textures. These features indicate rapid cooling during solidification throughout the lava flow. We interpret Unit 1 as a compound lava flow consisting of numerous individual flow units 0.1–10 m thick. The large number of thin flow units, together with the absence of sharp flow contacts, may indicate both (1) proximity to the eruptive vent and (2) rapid eruption of the entire lava flow. The observed decrease in maximum flow unit thickness upward in the lava may reflect an exponentially diminishing eruption rate with time.

Unit 1 is essentially aphyric. The groundmass consists of plagioclase, augite, magnetite, trace olivine, and mesostasis. Clay alteration is total for

[1]Duncan, R.A., Larsen, H.C., Allan, J.F., et al., 1996. *Proc. ODP, Init. Repts.,* 163: College Station, TX (Ocean Drilling Program).

[2]Shipboard Scientific Party is given in the list preceding the Table of Contents.

both mesostasis and olivines whereas plagioclases and augites are generally fresh. The textures vary between two extremes: (1) a very fine grained rock with quench textures of spherulitic, acicular, and skeletal plagioclases (and sporadic augites) within a vesicular and mesostasis-rich matrix and (2) a "normal" fine-grained intersertal, intergranular to variolitic and subophitic rock with large disseminated vesicles (up to 20% and up to 4 mm across). Both very sharp (internal flow boundaries) or gradational transitions occur between the quenched and normal textures.

Igneous Unit 2 is porphyritic with phenocrysts of plagioclase, augite, and trace olivine in a very fine grained matrix. Olivine phenocrysts occur as individual disseminated grains that are now totally altered to clay. Plagioclase and augite phenocrysts are fresh and commonly strongly zoned and resorbed (plagioclase) and occur in glomerocrystic clusters. The groundmass has a seriate texture defined by microphenocrysts of very elongate plagioclases (4%–5% of groundmass). Stubby olivines (trace to 2%) and anhedral augites (<1%) also form microphenocrysts. The groundmass (up to 0.2-mm grains) consists of plagioclase laths, equant augites, euhedral to skeletal magnetite, and mesostasis in an intersertal/intergranular to variolitic texture.

The two units recovered at Site 989 are both strongly depleted in a number of incompatible elements such as Zr, Nb, Ti, and P, and the original magma presumably melted from a depleted mantle source. Both lava flows are composed of evolved basalt, which implies crystal fractionation in a magma reservoir underlying this part of the volcanic succession. Similar crustal magma storage was invoked for the Site 917 Lower Series lavas, which have assimilated an Sr- and Ba-rich crustal component. The low Sr and Ba contents in the Site 989 lavas preclude direct correlation with the Lower Series at Site 917. In contrast, the lavas at Site 989 have either escaped crustal contamination or assimilated a crustal component different from that which contaminated the lavas at Site 917.

Physical properties measurements (*P*-wave velocity, bulk and grain densities, and porosity) of Unit 1 are quite constant with depth and correlate well between holes. The transition from Unit 1 to Unit 2 is clearly recognized, with the average *P*-wave velocity increasing from 5.2 to 6.0 km/s, density increasing from 2.8 to 3.0 g/cm^3, and porosity decreasing from 12% to 2%. The 3% average reduction between *P*-wave velocity measurements performed on minicores vs. split core sections may be due to drilling-induced fracturing of the outer edges of the cores.

Deformation of the cored sequence at Site 989 is principally in the form of brittle fracturing, manifest as veining and jointing. Veining is commonly present as two conjugate sets, one postdating the other, but both infilled with a combination of green clays and zeolites. Measured dips within Unit 1 for flow banding and other forms of textural variation, such as vesicular layers, are scattered but are concentrated between 15° and 45°. These features are interpreted to be chilled surfaces of flow units within a compound flow.

Preliminary shore-based studies confirm that Unit 1 recovered in both holes carries a steeply inclined normal magnetic polarity. This flow and two flows recovered at Site 990 are the first flows of normal polarity reported from the East Greenland margin. If Unit 1 is located stratigraphically below the Lower Series of Site 917, current stratigraphic evidence correlates the normal polarity event recorded by Unit 1 with Chron C27n or C28n (Fig. 8, "Introduction" chapter, this volume). Unit 2 appears to contain both normal and reversed polarity. The normal interval at the top of the flow was possibly remagnetized during the emplacement of the normally magnetized Unit 1. All discrete samples from Holes 989A and 989B, demagnetized to 80 mT and measured on the cryogenic magnetometer, carry normal polarity. Discrete samples from the lower part of Unit 2 contain reversed polarity.

BACKGROUND AND OBJECTIVES

Site 989 is located 43 km offshore of the East Greenland coast, within the southern drilling transect EG63 (Figs. 1, 2), and is one of the three drill sites planned for this transect (Fig. 3, "Introduction" chapter, this volume). Landward (west) of the EG63 transect, Precambrian basement is exposed within the high coastal mountains. Along the outermost coast the Precambrian crust is intruded by a few coast-parallel dikes of approximately vertical orientation. These are presumed to be of early Tertiary age and to have fed part of the early succession of lava flows in this area of the margin.

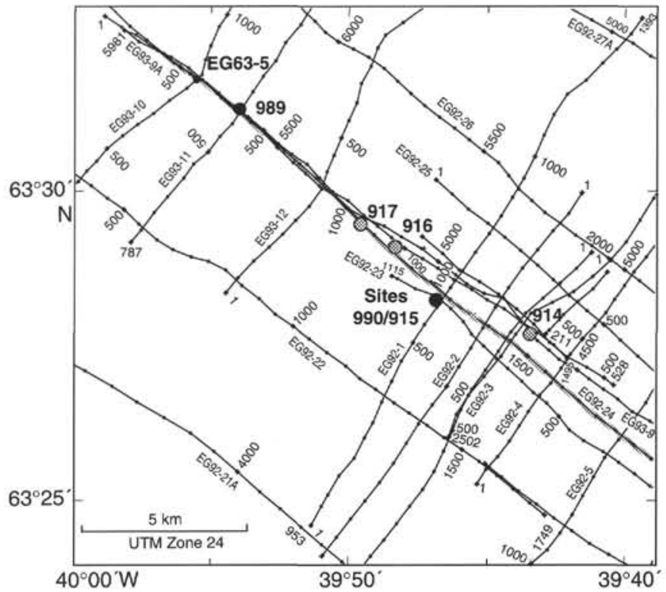

Figure 1. Location of Site 989 drill sites and site-survey data.

Geophysical data indicate that the Precambrian basement continues seaward for approximately 35 km. At this distance from the coast a continuous lava cover onlaps the basement from the southeast (Fig. 4, "Introduction" chapter, this volume, and Figs. 2, 3). The onlap zone is a monoclinal, seaward-facing flexure zone with the lavas dipping seaward (southeast) between 10° (uppermost part) and 25° (lowermost part; dip direction less well controlled). Landward-dipping normal faults are present within the flexure zone. The offshore lava sequence thickens seaward and is part of the featheredge of the Southeast Greenland SDRS. Seafloor-spreading Anomaly 24N is located approximately 150 km seaward of the site over the outermost part of the SDRS (Fig. 1, "Introduction" chapter, this volume). The main part of the SDRS lies landward of Anomaly 24N and is therefore assumed (Larsen and Jakobsdóttir, 1988; Larsen, Saunders, Clift, et al., 1994) to be of magnetic Chron C24r age (53–56 Ma; Berggren et al., 1995).

Within the flexure zone, the lava flows crop out at the seabed or subcrop below thin (5–10 m, locally up to 50 m) glaciomarine sediments in a zone approximately 5 km wide and comprise a stratigraphic thickness of about 1 km. Seaward the lavas are covered with progressively thicker postrift sediments of Eocene and younger age (Sites 915 and 916; Larsen, Saunders, Clift, et al., 1994). The lava sequence was cored at Leg 152 Site 917, and prerift metasediments with a steep to subvertical orientation were recovered at about 800 mbsf, from below the breakup unconformity (Larsen, Saunders, Clift, et al., 1994).

Site-survey data providing seismic cross lines through Site 989 and proposed Site EG63-5 (Fig. 3) have shown the existence of an acoustically layered sequence landward of Site 917. This seismically imaged unit is located below the lavas and the breakup unconformity. We interpret the unit as prerift sediments similar to those drilled at Site 917. However, the shallower dip of these possible prerift sediments at Site 989 is in strong contrast with the steep dip of the drilled prerift sediments at Site 917.

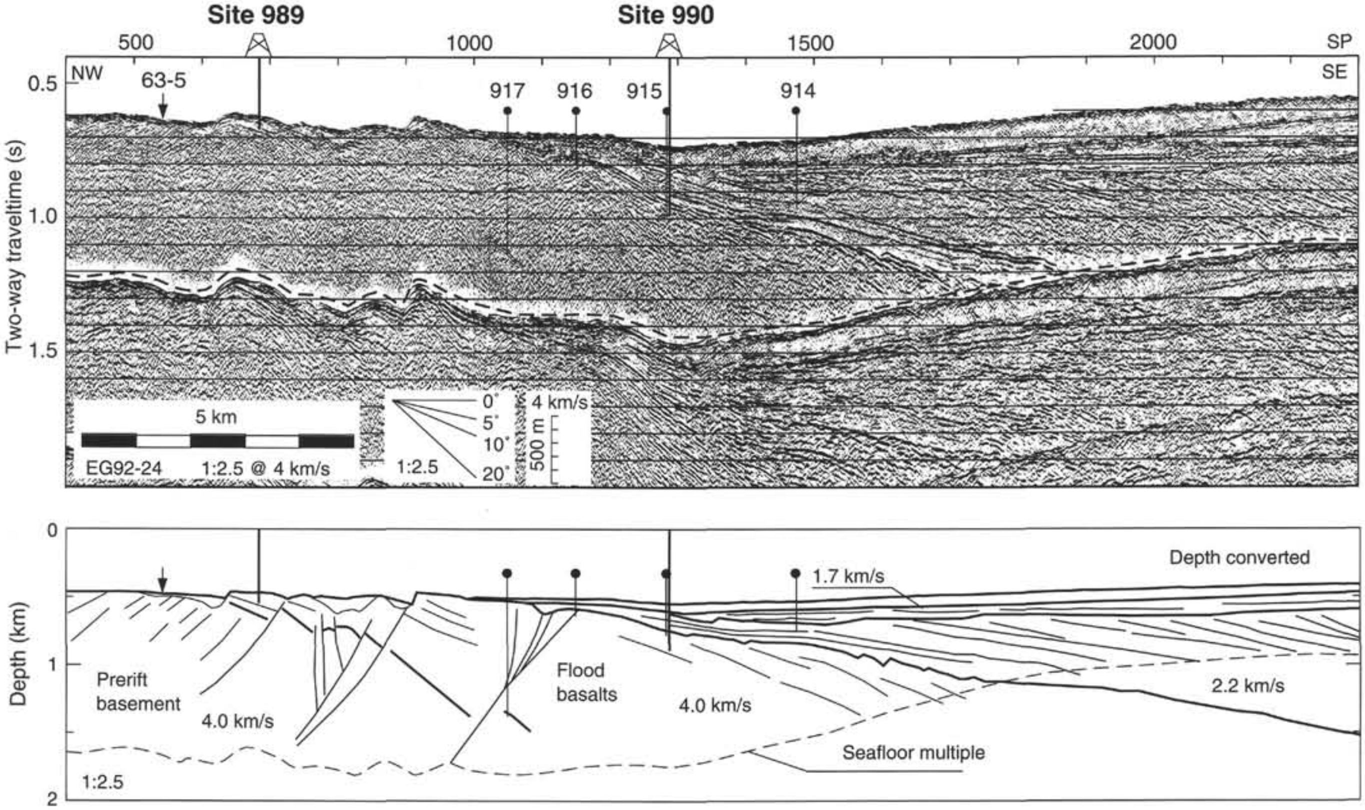

Figure 2. Seismic cross section through Site 989 (top). Interpretations are shown in the line drawing (middle) and migrated section (bottom). Steeply dipping to subvertical prerift sediments were encountered within the rotated fault block located below the lava sequence at Site 917. Sites 914–917 are described in Larsen, Saunders, Clift, et al. (1994). Seismic velocities used in the depth conversion are given in km/s.

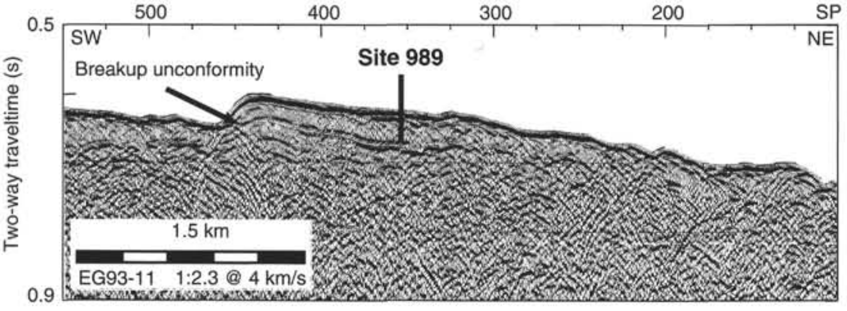

Figure 3. Seismic cross line through Site 989.

The lavas drilled at Sites 917 and 915 show development from initial continental volcanism (Lower and Middle Series lavas), through transient picritic volcanism, and into oceanic volcanism (Upper Series and younger lavas; see Fig. 2, "Introduction" chapter, this volume). Because of the normal faulting in the flexure zone, stratigraphic omission can be expected depending on drill site location. Therefore, drilling at Site 917 most likely did not sample significant portions of the deeper, oldest part of the Lower Series.

The Sites 917 and 915 lavas all show a reverse magnetic polarity (Larsen, Saunders, Clift, et al., 1994). The age of the Lower and Middle Series has been established radiometrically at about 61 Ma (Sinton and Duncan, in press), suggesting a correlation with magnetic Chron C26r or C27r (Berggren et al., 1995). A significant hiatus (61 to 56 Ma) may be present between the Middle Series and the Upper Series, if the main SDRS lava flows are restricted to magnetic Chron C24r age.

Site 989 is located at a water depth of 459.5 m, within the lowermost part of the lava sequence that crops out at the seabed (Figs. 1, 2). At the drill site, only thin (5 m) glaciomarine sediments cover the volcanic series. The uppermost lava unit dips gently seaward at approximately 10° and shows an acoustically transparent interior with a well-defined bottom as deep as 100 mbsf (depending on the seismic velocities applied).

The main objective of drilling at Site 989 was to penetrate and sample these oldest lavas of the SDRS complex along the EG63 transect and to investigate the breakup unconformity and the underlying, layered upper crust of supposedly prerift sediments. Important goals were to determine the age and nature of the breakup unconfor-

Table 1. Site 989 coring summary.

Core	Date (Sept. 1995)	Time (UTC)	Depth (mbsf)	Length cored (m)	Length recovered (m)	Recovery (%)
163-989A-						
1R	17	0530	0.0–9.0	9.0	5.49	61.0
2R	17	0900	9.0–14.3	5.3	4.68	88.3
3R	17	1420	14.3–21.4	7.1	5.85	82.4
Coring totals:				21.4	16.02	74.9
163-989B-						
		Drilled from 0.0 to 4.0 mbsf				
1R	18	0700	4.0–9.2	5.2	4.61	88.6
2R	18	1300	9.2–14.2	5.0	4.29	85.8
3R	18	1630	14.2–15.9	1.7	1.70	100.0
4R	18	2020	15.9–20.8	4.9	4.96	101.0
5R	19	0115	20.8–25.8	5.0	4.66	93.2
6R	19	0710	25.8–35.5	9.7	10.01	103.2
7R	19	1215	35.5–45.1	9.6	9.23	96.1
8R	19	1515	45.1–54.7	9.6	9.10	94.8
9R	19	1800	54.7–64.4	9.7	10.01	103.2
10R	19	2100	64.4–74.1	9.7	9.16	94.4
11R	20	0315	74.1–77.1	3.0	2.46	82.0
12R	20	0845	77.1–78.6	1.5	1.10	73.3
13R	20	1415	78.6–83.6	5.0	2.55	51.0
14R	20	1545	83.6–84.2	0.6	0.12	20.0
Coring totals:				80.2	73.96	92.2
Drilled:				4.0		
Total:				84.2		

mity, the prerift history, and the nature and composition of the early rift volcanism. An additional objective of the site was to sample material suitable for precise age determination by $^{40}Ar/^{39}Ar$ methods to further establish the timing of the onset of the East Greenland volcanism.

OPERATIONS

After a series of repairs to our top drive and related rig hardware in Reykjavik, Iceland, we transited back to the more southerly EG63 transect (Fig. 3, "Introduction" chapter, this volume). A brief 3.5-kHz survey was completed over the site along the track of seismic line GGU/EG92-24/1, which covers proposed Sites EG63-6 and EG63-5. Consistent with the pre-cruise site-survey data, the seismic record suggested that 5–10 m of sediment lies on top of the lava flow sequence, which would be sufficient to allow spudding in of the RCB. A coring summary of this site is given in Table 1.

Hole 989A

The beacon marking the site was dropped by Global Positioning System coordinates at 1445 UTC on 16 September. The beacon prereleased, requiring deployment of a second beacon. The strong southerly current in the area caused the second beacon to drift 150 m aft of the deployment point. Because of the shallow water in the region (459.5 m), it was necessary to offset north of location and drop a third beacon at 1455 UTC. This deployment was successful.

Because of the nearly hard-rock spudding, a shorter and more flexible six-collar bottom-hole assembly (BHA) utilizing a mechanical bit release was used. The initial sediment penetration was made without the benefit of the video camera, and Hole 989A was spudded at 2000 UTC at 63°31.355′N, 39°54.113′W. After quickly drilling 3 m, the rate of penetration dropped significantly. Recovery of the first core revealed that a large, gneissic glacial erratic boulder had been cored, followed by massive basalt.

Another two cores were drilled to 21.4 mbsf before an iceberg forced the ship to abandon operations. At 1100 UTC on 17 September, an iceberg estimated to be 100 m wide and 15 m high approached within 6.3 km of the vessel. The *Gadus Atlantica* was then directed to attempt to tow the iceberg away from *JOIDES Resolution.* After the first attempt at towing the iceberg failed, instructions were given to the drilling crew to deploy a free-fall funnel. The *Gadus Atlantica* was unable to snare the iceberg with a towing line after four attempts.

With the iceberg at a distance of 2.8 km and closing at 1–2 kt, coring was suspended and the bit raised to 14 mbsf. Attempts to lasso the iceberg possibly influenced the course of the iceberg, which suddenly appeared to change course toward *JOIDES Resolution.* The sudden change in the path of the iceberg surprised the drilling crew, who were unable to pull out of the hole with the drill pipe because the elevators and rotary bushing had been set back in preparation for the funnel deployment. With the iceberg at 0.9 km, the captain gave instructions to offset the vessel 800 m astern, dragging the BHA and bit out of the hole. The iceberg passed within 10 m of *JOIDES Resolution* and cleared the vessel to port.

The core barrel was retrieved with no difficulty or drag, which implied that the drill string was not bent. The bit was tripped to the surface, and the drill string and BHA were inspected and found to be in good condition. A new, harder formation C-7 bit was then substituted for the C-4 bit, and three additional drill collars were added to the BHA to add weight.

Hole 989B

An attempt was then made to reenter Hole 989A. Although the iceberg prevented us from deploying a free-fall funnel, the Hole 989A crater was easily detected with the video camera, because dragging the BHA out of the hole had created a noticeable furrow leading away from the hole. After several unsuccessful attempts to reenter Hole 989A, Hole 989B was spudded at 2400 UTC on 17 September at 63°31.355′N, 39°54.110′W. The hole was then washed down to 4 mbsf, where contact was made with basalt.

Because of the light weight on bit (2–4 klb), the first core took 420 min to advance 5.2 m. When the barrel was retrieved, it contained 4.6 m of basalt. Continuous rotary coring then advanced slowly but with spectacular recovery to 74 mbsf (97% of the cored interval), where the basalt noticeably hardened and recovery lowered.

A free-fall funnel was deployed when the depth of the hole reached 21 mbsf. After 52 hr of rotation were accumulated, the drill string was tripped to the surface from 84 mbsf to change the bit. The

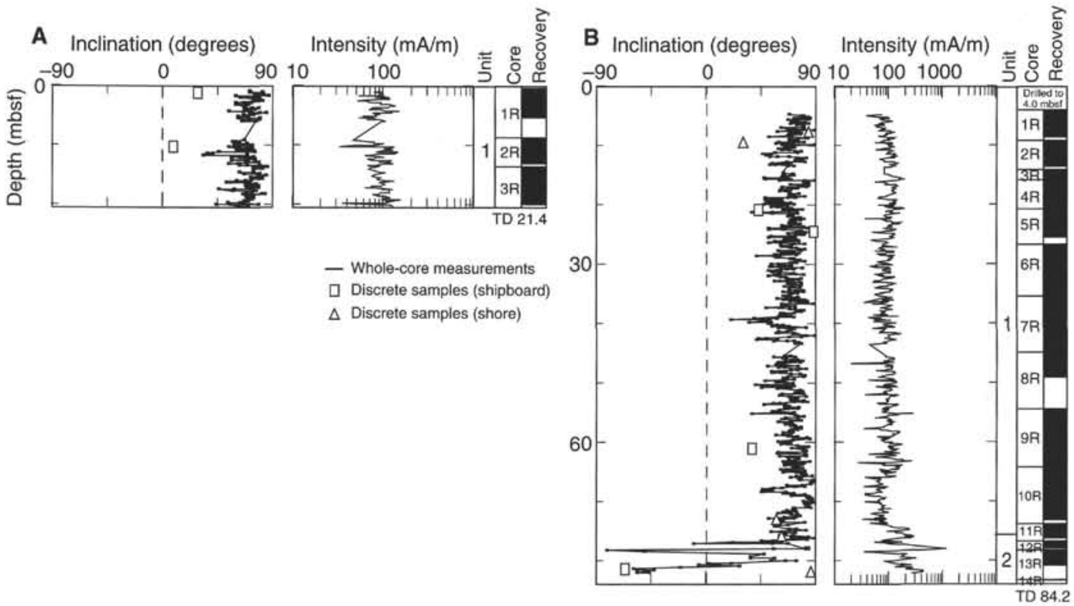

Figure 4. The magnetostratigraphy obtained from Holes 989A (**A**) and 989B (**B**) showing the variation in inclination and intensity after demagnetization at 30 mT.

video camera was deployed to observe the retraction of the drill bit out of the hole to ensure that the free-fall funnel was not moved during the process.

Instead of replacing the bit and reentering Hole 989B, it was decided to temporarily cease operations at this site and move to the next site. This was done because northwest winds were driving ice within 7.4 km of the site. The forecast from the Danish Meteorological Institute indicated that strong winds were expected to continue from this sector for the next couple of days, which implied that the ice threat would only increase at this location. At 1930 UTC on 20 September, the vessel was dynamically offset 9 km to the southeast to begin operations at Site 990.

LITHOSTRATIGRAPHY

The sedimentary sequence at Site 989 was not recovered in any coherent way by coring, but several other lines of evidence suggest that the thin sediment cover at Site 989 should be considered a single lithologic unit (lithologic Unit I). Seismic profiles across Site 989 and the driller's log from the site indicate a sediment thickness of approximately 4 m, and sediment characteristics appear homogeneous throughout this interval. The only material recovered from lithologic Unit I consists of discrete rock fragments. In Hole 989A, these are a 51-cm-long sequence of gneiss fragments (labeled Section 163-989A-1R-1 [Pieces 1 through 3]) and a 5-cm-long piece of fine-grained to aphyric basalt (labeled Section 163-989A-1R-1 [Piece 4]). In Hole 989B, these are a 22-cm-long sequence of fragments of aphyric basalts and metabasalts, quartzite, and dolerite (labeled Section 163-989B-1R-1 [Pieces 1 through 3]). The lithologies of these clasts are consistent with the lithologies of ice-rafted material recovered at Site 988 and during Leg 152; as a result, the clasts recovered at Site 989 are also interpreted as ice-rafted erratics, even though they were not recovered within a finer grained matrix. In comparison with the glacial tills and the glaciomarine sediments drilled at the shelf sites during Leg 152, the drilling conditions within the sediments at Site 989 suggest that these are glaciomarine deposits, rather than overcompacted glacial tills.

PALEOMAGNETISM

Paleomagnetic studies at Site 989 (Holes 989A and 989B) included analyses of the NRM and anhysteretic remanent magnetization (ARM) using the whole-core cryogenic magnetometer and the magnetic susceptibility using the multisensor track. Split core Sections 163-989A-1R-1 through 3R-5 (igneous Unit 1) and 163-989B-1R-1 through 14R-4 (igneous Units 1 and 2) were demagnetized in 10-mT steps up to 30 mT to remove the low-coercivity components, thought to be induced by the drilling process. Their removal reduced intensities to between 1% and 20% of the NRM values.

Unit 1 of Holes 989A and 989B carries a normal magnetic polarity with a mean inclination of 68° (Table 2 on the CD-ROM in the back pocket of this volume; Fig. 4). This flow and two flows from Site 990 represent the first flows of normal polarity reported from the East Greenland margin (Larsen, Saunders, Clift, et al., 1994; Soper et al., 1976). If the Site 989 lavas are older than the Site 917 lavas, current stratigraphic evidence (Sinton et al., 1994; Sinton and Duncan, in press) suggests that this normal event correlates with Chron C27n or perhaps C28n. Unit 2 appears to contain both normal and reversed polarity. The normal polarity interval at the top part of the flow was probably remagnetized during emplacement of the overlying normally magnetized Unit 1. Discrete samples from Hole 989A and from Cores 163-989B-1R through 11R (Unit 1 and top of Unit 2) carry a normal polarity after demagnetization to 80 mT. Discrete samples from Cores 163-989B-11R through 14R (lower part of Unit 2) contain a reversed polarity after partial demagnetization. Because the shipboard spinner magnetometers were out of order and the results of discrete-sample measurements on the cryogenic magnetometer were inconclusive, additional demagnetization measurements were conducted after the cruise. The preliminary shore-based data confirm the existence of the normal polarity interval in basalts from Hole 989B (Table 3 on the CD-ROM on the back pocket of this volume).

The bulk magnetic susceptibility of the Unit 1 samples was 10^{-2} SI, whereas those of Unit 2 had approximately one-half that value. The bulk magnetic susceptibility values can be used to calculate the Koenigsberger ratio, defined as $Q = M/kH$, where M = NRM, k = bulk magnetic susceptibility, and H = the Earth's present-day magnetic

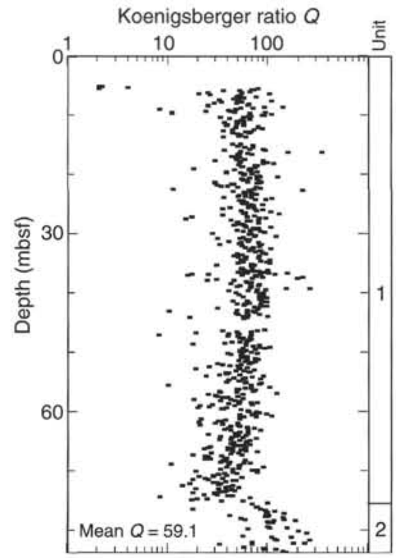

Figure 5. Variation of Koenigsberger ratio (Q ratio) vs. depth for material recovered from Hole 989B.

field at the sampling locality (estimated at 54 µT; Merrill and McElhinny, 1983). The mean Q value of flows from Hole 989B is 59.1 (Fig. 5), which implies that the remanent magnetization dominates the induced magnetization and that the surface magnetic anomaly at the site provides a reliable record of the original magnetic polarity of the ocean floor. The ARM measurements of selected discrete samples imply that the remanent magnetization is isotropic, which suggests that the basalts of Units 1 and 2 are reliable paleomagnetic indicators.

STRUCTURAL GEOLOGY

Deformation within the igneous units cored at Site 989 was principally in the form of brittle fracturing, manifested as veining and jointing. Veining is most densely developed in the more massive parts of the thick igneous Unit 1, toward the top of the drilled sequence at Site 989, in comparison with the thinner Unit 2 below 73.2 mbsf. Veining is commonly present as two conjugate sets (Fig. 6), one postdating the other, but both filled by a combination of green clays, zeolites, and calcium carbonate. Measurements of the orientation of all planar veins in the recovered material do not show a preferred dip direction (Fig. 7). The measured dips for flow banding and other semiplanar igneous textures, such as vesicular layers, cluster between 15° and 45° (Fig. 8). Such features are most common in the upper part of Unit 1 and sparse near the bottom of that unit. These vesicular and finer grained layers are interpreted to be chilled tops of internal flow lobes that were subsequently buried by later eruptions during the buildup of the thick (compound flow?) Unit 1 (see "Igneous Petrology" section, this chapter). The fact that seismic surveys show reflectors (i.e., general bedding of the lava pile) that dip ≤10° around Site 989 (see "Background and Objectives" section, this chapter) suggests that the igneous structures measured in the core were not originally subhorizontal. However, the measured steep dips are consistent with the local construction of a volcanic edifice (see "Igneous Petrology" section, this chapter). The apparent increase in dip upsection above 53 mbsf (see Fig. 8) is also consistent with the growth of a volcanic pile, because these typically form on an originally flat surface and build up into a cone with gradually increasing slopes with time. All structural features measured in the archive half

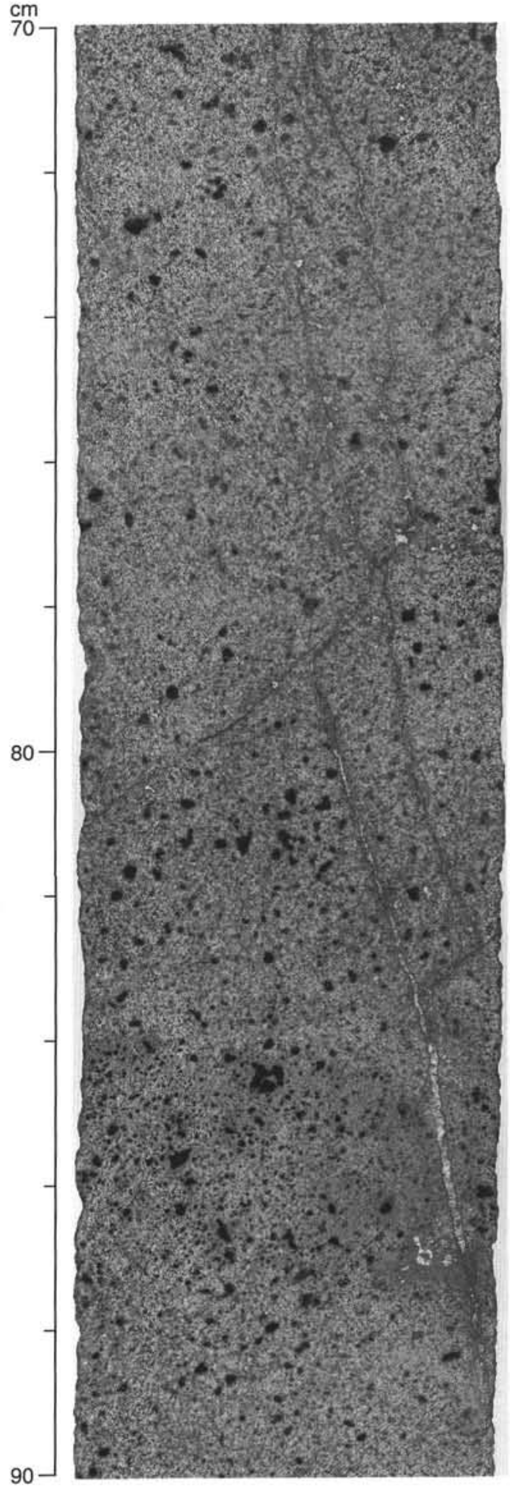

Figure 6. Photograph of conjugate vein sets at Section 163-989B-6R-2, 70–90 cm. The steeper set is cut by the shallower set. The steeper veins are filled by clay lining and zeolites, whereas the shallower set appears to be only clay filled. Zeolite-filled vesicles are adjacent to the veins.

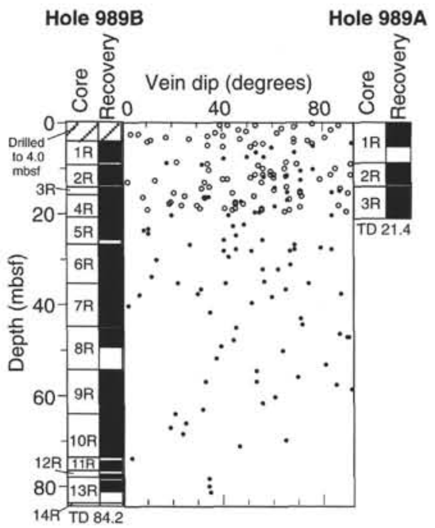

Figure 7. Variation in the dip of veins measured in core from Site 989. Open circles denote data from Hole 989A and solid circles show data from Hole 989B.

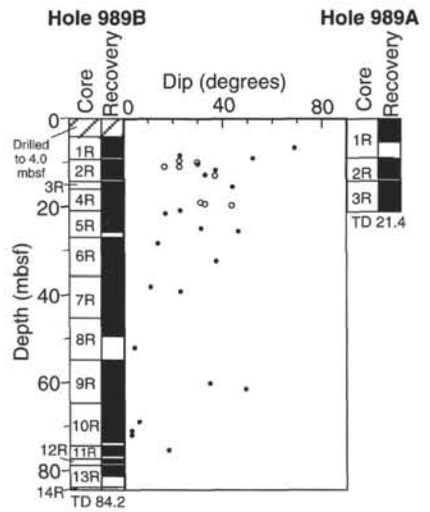

Figure 8. Variation in the dip of flow banding and other semiplanar textures, such as vesicular layers, measured in core from Site 989. Symbols as for Figure 7.

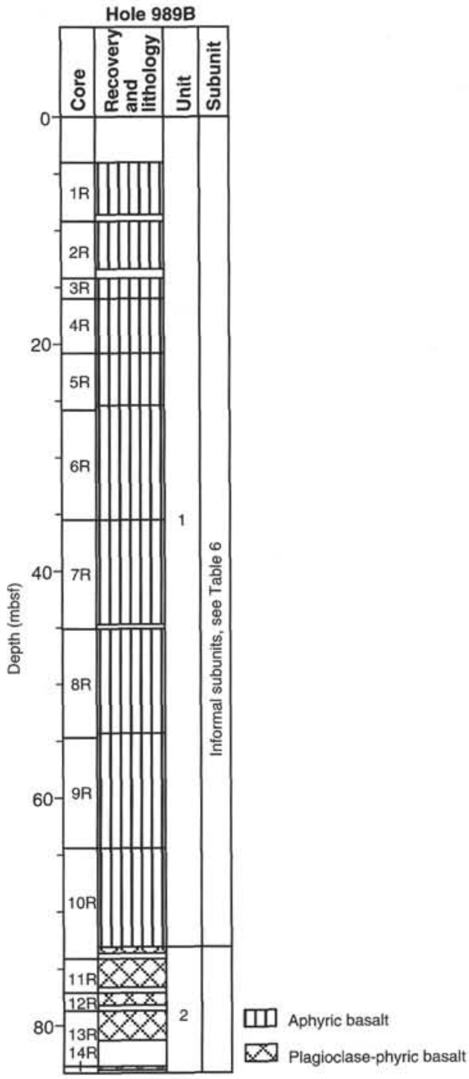

Figure 9. Coring and lithologic summary for Site 989. Cores 163-989B-6R and 9R had recovery greater than 100% (perhaps because of tidal variations) and were consequently pushed up into the range of the previous cores, giving total recovery of these cores close to 100%.

of the core are recorded in Tables 4 and 5 on the CD-ROM in the back pocket of this volume.

IGNEOUS PETROLOGY

Lithology

Two holes were drilled at Site 989. Hole 989B was situated immediately adjacent to Hole 989A to core the same material, and it reached a significantly greater depth (84.2 vs. 21.4 mbsf). Drilling data indicate that the sediments at Site 989 are approximately 4 m thick, and the top of the igneous succession was consequently placed at 4 mbsf at both locations. Igneous rocks were cored from 4 mbsf to the bottom of the holes. The recovered section consists of two igneous units (Fig. 9).

Unit 1 is a gray, vesicular, moderately altered aphyric basalt. It is at least 69 m thick, and recovery of this unit was very high (~93%). The upper contact is not preserved. The lower contact is assumed to lie at 73.2 mbsf, just below Section 163-989B-10R-7 (Piece 6, 92 cm), which is a microcrystalline basalt with many small (<5 mm diameter) vertical pipe vesicles (Fig. 10). Unit 1 contains an average of 5%–10% vesicles throughout the upper 55 m, with local variation from 0% to 15%. Vesicles are commonly lined with dark greenish gray clay, and those near veins are filled with zeolite.

Unit 1 contains repeated bands with textural variations interpreted as quenched tops of pahoehoe flow lobes within the unit (locations are tabulated in Table 6). A flow lobe top is characterized by a distinct textural succession, consisting of a 1–2-cm finely crystalline band with a bimodal distribution of vesicle sizes, immediately underlain by a 2–6-cm zone of dense (relatively nonvesicular) lava that grades downward into regions of average (5%–10%) vesicularity (Fig. 11). Illustrations of these textural features can be found in the scanned images for Hole 989B on the CD-ROM that accompanies this volume. Flow tops occur at spacings between 0.1 and 10 m. The thicknesses of the individual flows within Unit 1 are shown in Figure 12. The maximum subunit thickness markedly increases and the number of very thin (<1 m) subunits decreases downward in the unit.

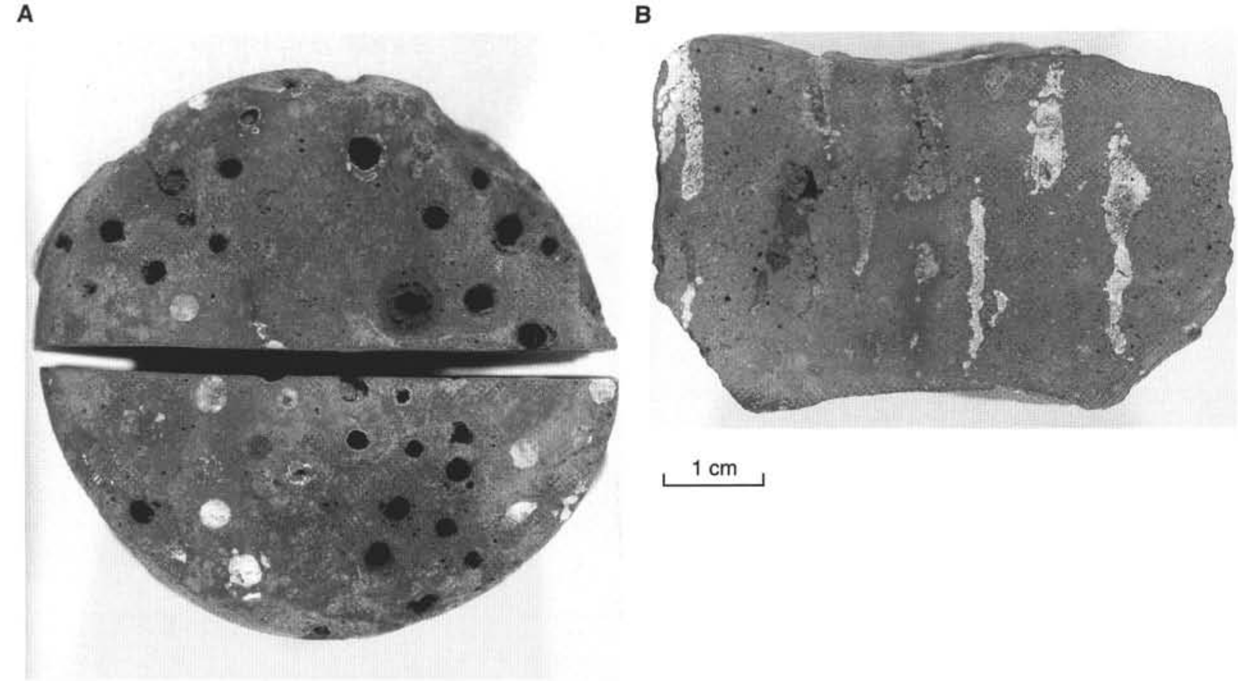

Figure 10. Vertical pipe vesicles at the lower contact of Unit 1 in Section 163-989B-10R-7, 87–92 cm, shown in both horizontal (**A**) and vertical (**B**) views.

There is a good correlation between the position of the subunit tops in Holes 989A and 989B.

Unit 2 was cored from 73.2 mbsf to the bottom of the hole, at 84.2 mbsf. It is thus at least 11 m thick. The top is not preserved. It is a massive gray, moderately altered, sparsely to moderately plagioclase-phyric basalt with a microcrystalline groundmass and very few vesicles. Vesicles occur only throughout the upper 6–7 m of the unit in rounded and commonly elongate segregation patches that are 1–5 cm across. The individual vesicles are commonly irregular in shape and are filled with greenish gray clay. The overall flow morphology and the nature of the segregated patches are similar to flows identified as aa in Hole 990A.

Identifiable brecciated and/or oxidized zones that commonly define the tops of flow units were not recovered from either unit at Site 989. Although the thickness of the material missing from Unit 1 is not known, a maximum of 0.5 m is missing from the top of Unit 2. Unit 2 shows no signs of oxidation or vesiculation toward the top (common features in subaerial flows), nor are there any preserved features indicative of subaqueous emplacement. However, the compound-flow morphology and the constant vesicularity observed in Unit 1 are most likely subaerial features.

Primary Mineralogy and Texture

Unit 1 is an aphyric basalt with rare scattered plagioclase glomerocrysts (seen in three of the 12 thin sections). The groundmass consists of plagioclase (38%–50%), augite (21%–40%), magnetite (mostly 1%–4%), olivine (trace to 1%), and mesostasis (10%–39%). Alteration to clay is complete for both mesostasis and olivine. Plagioclase and augite are fresh with alteration along some grain boundaries and cleavage planes. Zoning is ubiquitous within both plagioclase and augite. The magnetite grains are usually homogeneous and unexsolved. Separate ilmenite crystals were not observed. The rock textures vary between two extremes: (1) a microcrystalline rock with quench textures of acicular and skeletal plagioclase (rare augite and magnetite; Figs. 13, 14) within a vesicle- and mesostasis-rich matrix and (2) a more typical fine-grained intersertal to subophitic rock (Fig. 15) with large disseminated vesicles (up to 20% and up to 4 mm in diameter). Both sharp and gradational transitions occur between quench and normal textures.

Unit 2 is slightly to moderately porphyritic with phenocrysts of plagioclase (2%–3%), augite (1%–2%), and olivine (trace to 2%) in a microcrystalline matrix. Only the plagioclase phenocrysts are visible in hand specimen. Olivine phenocrysts, completely altered to clay, occur as individual disseminated grains, whereas plagioclase and augite phenocrysts commonly occur together in glomerocrystic clusters. Plagioclase and augite are fresh, usually strongly zoned, and the plagioclase cores are commonly resorbed. The groundmass has a seriate texture defined by microphenocrysts (0.2–0.8 mm) of very elongate plagioclase (4%–5% of the groundmass). Stubby olivine (trace to 2%) and anhedral augite (<1%) also form microphenocrysts. The groundmass (up to 0.2-mm grains) consists of plagioclase laths (34%–40%), equant augite (30%–42%), euhedral to skeletal magnetite (3%–4%), and mesostasis (15%–16%) with an intersertal to intergranular texture.

Major Oxide and Trace-element Composition

Major oxide and selected trace-element compositions of eight basalt samples from Site 989 were determined by shipboard X-ray-fluorescence analysis. The analytical data for the seven basalt samples recovered from Unit 1 in Holes 989A and 989B and one sample from Unit 2 are presented in Table 7 together with an analysis of a typical basalt sample from the Lower Series at Site 917 for comparison.

To assess the effects of secondary alteration, Sample 163-989B-2R-1, 83–88 cm, was prepared by two different methods. The first split was prepared by the normal crushing and cleaning procedures (see "Igneous Petrology" section, "Explanatory Notes" chapter, this volume). The second split was first crushed to sand size and subjected to extreme ultrasonic cleaning to remove clay particles. Both the cleaned residue and the clay fraction were analyzed, and the results are presented in Table 7. There are no significant differences in composition between the whole-rock and cleaned samples, except perhaps a modest reduction in Rb for the "ultracleaned" split.

Table 6. Location and thicknesses of internal boundaries within Unit 1 that have been interpreted as the tops of successive flow lobes.

Core, section, piece	Top (mbsf)	Length recovered (m)	Length curated (m)	Flow top (mbsf)	Flow thickness (m)
163-989B-					
1R-2 (Piece 1B)	4	4.61	5.42	5.47	
1R-3 (Piece 1A)				6.66	1.19
1R-3 (Piece 1B)				6.83	0.17
1R-3 (Piece 5)				7.51	0.68
1R-4 (Piece 5)				8.58	1.07
1R-4 (Piece 7)				8.84	0.26
1R-4 (Piece 9)				9.31	0.47
2R-1 (Piece 4)	9.2	4.29	4.3	9.68	0.37
2R-1 (Piece 5)				10.28	0.60
2R-2 (Piece 1A)				10.52	0.24
2R-2 (Piece 1C)				11.44	0.92
2R-3 (Piece 1)				11.85	0.41
2R-4 (Piece 1A)				12.17	0.32
2R-4 (Piece 1A)				12.43	0.26
2R-4 (Piece 1A)				12.79	0.36
2R-4 (Piece 1B)				13.05	0.26
2R-4 (Piece 1B)				13.32	0.27
3R-1 (Piece 4D)	14.2	1.7	1.48	14.67	1.35
3R-1 (Piece 4E)				15.08	0.41
3R-1 (Piece 4F)				15.39	0.31
4R-2 (Piece 1A)	15.9	4.96	4.99	17.57	2.18
4R-3 (Piece 1B)				19.33	1.76
4R-4 (Piece 1A)				20.05	0.72
5R-1 (Piece 1B)	20.8	4.66	4.92	21.70	1.65
5R-2 (Piece 2)				22.55	0.85
5R-2 (Piece 3B)				23.29	0.74
5R-3 (Piece 3)				24.36	1.07
5R-4 (Piece 2)				25.26	0.90
6R-1 (Piece 1)	25.8	10.01	10.81	25.88	0.62
6R-1 (Piece 1)				25.96	0.08
6R-1 (Piece 5)				26.65	0.69
6R-2 (Piece 3B)				28.05	1.40
6R-2 (Piece 4)				28.44	0.39
6R-3 (Piece 2B)				29.30	0.86
6R-3 (Piece 3)				29.52	0.22
6R-4 (Piece 2)				30.45	0.93
6R-4 (Piece 3)				30.88	0.43
6R-6 (Piece 2)				33.77	2.89
6R-7 (Piece 1C)				34.41	0.64
6R-8 (Piece 1A)				35.39	0.98
6R-8 (Piece 2)				35.79	0.40
7R-2 (Piece 3)	35.5	9.23	9.5	37.60	1.81
7R-2 (Piece 3)				37.63	0.03
7R-2 (Piece 3)				38.36	0.73
7R-3 (Piece 1)				39.43	1.07
7R-4 (Piece 1A)				40.00	0.57
7R-4 (Piece 1A)				40.10	0.10
7R-5 (Piece 1A)				40.85	0.75
7R-6 (Piece 1)				41.88	1.03
7R-8 (Piece 1)				44.86	2.98
8R-1 (Piece 2A)	45.1	9.1	9.27	45.60	0.74
8R-1 (Piece 2A)				45.94	0.34
8R-2 (Piece 1B)				47.10	1.16
8R-2 (Piece 1B)				47.82	0.72
8R-3 (Piece 1C)				48.75	0.93
8R-3 (Piece 1D)				49.15	0.40
8R-4 (Piece 1A)				49.46	0.31
8R-4 (Piece 1C)				49.87	0.41
8R-4 (Piece 2)				50.13	0.26
8R-4 (Piece 2)				50.49	0.36
8R-6 (Piece 1A)				51.84	1.35
9R-2 (Piece 1)	54.7	10.1	10.01	57.02	5.18
9R-3 (Piece 1A)				57.55	0.53
9R-3 (Piece 1B)				57.98	0.43
9R-3 (Piece 1C)				58.49	0.51
9R-4 (Piece 1)				59.06	0.57
9R-4 (Piece 2C)				60.25	1.19
10R-5 (Piece 1D)	64.4	9.16	9.36	70.43	10.18
10R-7 (Piece 4)				73.16	2.73

Note: See text for identification criteria.

Unit 1 is basaltic in composition and has an evolved character, as indicated by the Mg# of 54–57 and low Ni (74–83 ppm) and Cr (43–52 ppm) (Table 7). The unit is also distinctive in its low concentrations of Sr and of the incompatible elements Nb, Zr, Y, and TiO_2 (Fig. 16). Analyses from all portions of Unit 1 are identical within analytical uncertainties, supporting the interpretation that all flow lobes identified in Unit 1 are part of a single eruptive event. The single analysis of Unit 2 is broadly similar in composition to Unit 1, but it is slightly more primitive, as indicated by the higher Mg# (57) and

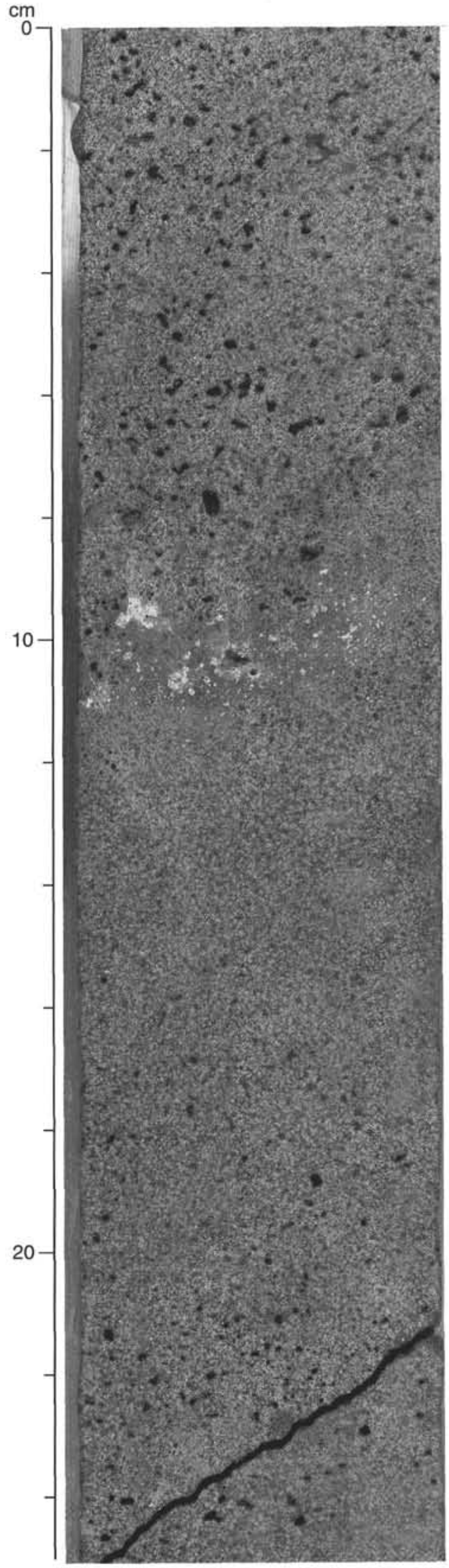

Figure 11. Top of flow lobe in Unit 1, Section 163-989B-2R-2, 0–25 cm. Note the zeolite-filled vesicles within the finely crystalline flow boundary and the abrupt change in vesicularity across the boundary.

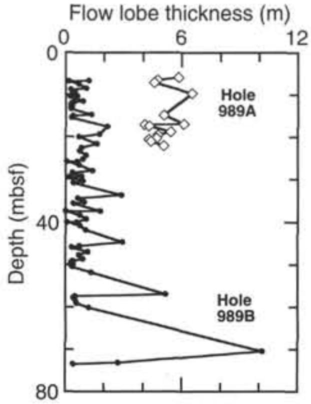

Figure 12. Thickness vs. depth of internal flow lobes within the compound lava flow of Unit 1 at Site 989. Note the correlation between Holes 989A and 989B, with data from Hole 989A offset 4 m in thickness for clarity.

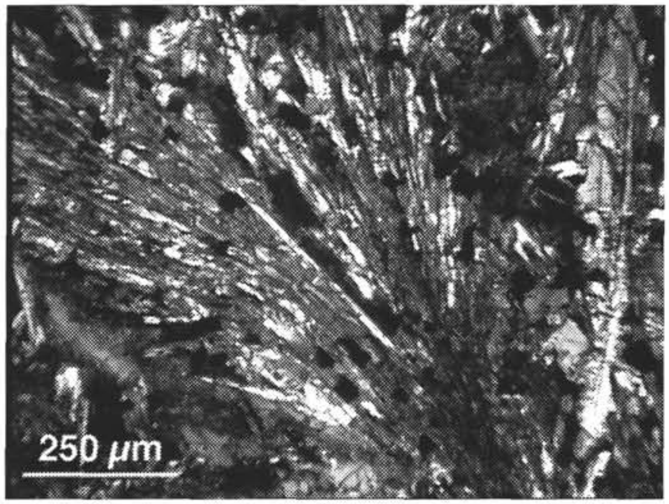

Figure 14. Variolitic texture in a quench band at the top of an internal flow unit contact in the compound lava flow of Unit 1. Scanned image of thin-section Sample 163-989B-6R-2, 133–136 cm.

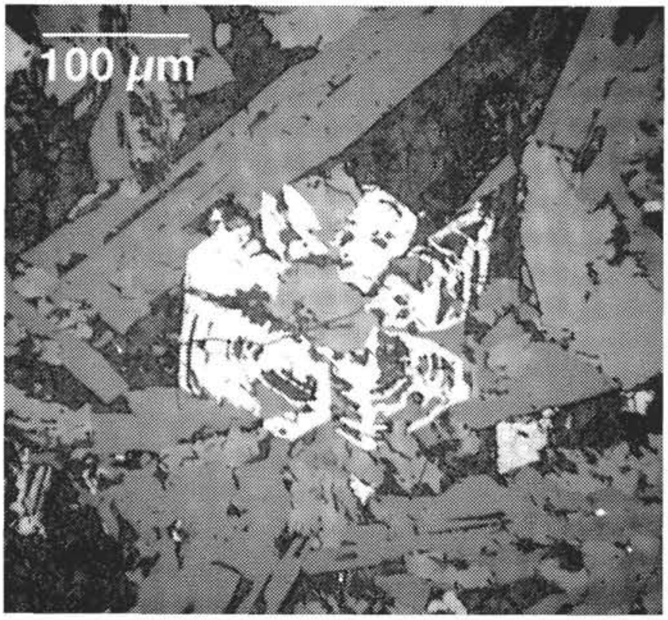

Figure 13. Skeletal magnetite in a quench band at the top of an internal flow unit contact in the compound lava flow of Unit 1. Scanned image of thin-section Sample 163-989B-7R-4, 43–47 cm.

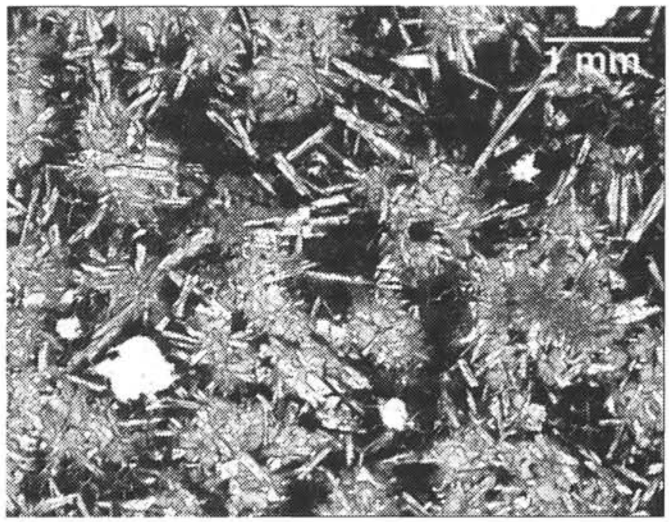

Figure 15. Intersertal texture, the common texture in the major part of the compound lava flow of Unit 1. Scanned image of thin-section Sample 163-989B-6R-2, 133–136 cm.

higher concentrations of Ni (98 ppm) and Cr (238 ppm). The evolved character of the basalts suggests storage and crystal fractionation of more primitive magmas before eruption.

The objective of drilling at Site 989 was to recover parts of the oldest SDRS. Based on seismic studies of the area (Larsen, Saunders, Clift, et al., 1994) the units drilled at Site 989 are interpreted to lie stratigraphically below the succession at Site 917, although there is a possibility of direct overlap because of faulting at Site 917. The analyses from Site 989 are compared with analyses of lavas from both the Site 917 Lower Series and the more seaward Site 918 in the multiple-element plot of Figure 17. The contrast between the Site 989 lavas and Site 917 Lower Series lavas is striking, particularly in the much lower Sr and Ba contents of the Site 989 lavas (see also Fig. 16). Based on these preliminary analyses, there is no compositional overlap between the successions at the two sites and thus the basalts at Site 989 have an origin and/or evolution different from those at Site 917.

Figure 17 shows that despite their position closest to land, the basalts at Site 989 are more similar to the oceanic succession at Site 918 than to the continental succession at Site 917. The basalts from Sites 989 and 918 have similar low ranges of the immobile elements Nb, P, Zr, Ti, and Y and slightly positive slopes of the P-to-Y curve segments. This implies slightly larger degrees of melting, perhaps at lower pressures, than for the Site 917 basalts.

Concentrations of the elements Rb, Ba, K, and Sr on the left side of Figure 17 must be interpreted with caution because of their mobility during alteration. However, the patterns are more consistent than would be expected had these elements been grossly affected by alteration processes. Relatively high Rb, Ba, and K may indicate crustal contamination, but the Site 989 basalts do not show the large positive

Table 7. Major oxide (wt%) and trace-element (ppm) analyses of basalts from Sites 989 and 917.

Hole:	163-989A	163-989A	163-989B	163-989B	163-989B	163-989B	163-989B	163-989B	163-989B	163-989B	152-917A
Core, section:	1R-4	3R-6	1R-4	2R-1	2R-1	2R-1	6R-2	10R-2	10R-7	12R-1	101R-4
Interval (cm):	82–87	39–42	115–119	83–88	83–88	83–88	57–60	3–7	55–59	92–96	81–85
Piece:	1B	1B	8	5	5	5	2B	1	5A	8C	—
Unit:	1	1	1	1	1	1	1	1	1	2	92
Depth (mbsf):	4.4	20.2	9.1	10.0	10.0	10.0	27.7	65.9	73.3	78.0	
				Whole rock	Cleaned	Clay					
Major oxides											
SiO_2	50.09	50.07	50.11	50.33	49.50	47.60	49.88	49.75	50.40	50.20	50.24
TiO_2	1.03	1.06	1.09	1.05	1.08	0.66	1.08	1.02	1.10	0.91	1.16
Al_2O_3	13.51	13.33	13.39	13.45	13.06	7.08	13.42	13.42	13.50	14.05	16.24
Fe_2O_3(t)	13.68	14.08	13.84	13.51	12.79	20.35	13.99	13.75	14.03	12.17	9.49
MnO	0.22	0.23	0.23	0.23	0.24	0.22	0.23	0.21	0.22	0.22	0.20
MgO	7.39	7.42	7.27	7.52	7.65	10.95	7.50	8.19	7.85	8.02	8.13
CaO	11.50	11.37	11.45	11.34	12.10	3.05	11.71	11.28	10.90	12.73	12.55
NaO	1.89	1.90	1.86	1.88	1.71	2.84	1.84	1.81	1.91	1.67	2.24
K_2O	0.28	0.29	0.28	0.29	0.29	0.31	0.24	0.25	0.29	0.25	0.19
P_2O_5	0.07	0.08	0.07	0.07	0.07	0.21	0.09	0.05	0.08	0.05	0.13
Total	99.66	99.83	99.59	99.67	98.49	93.27	99.98	99.73	100.28	100.27	100.53
LOI	0.12	0.53	0.41	0.65	0.22	6.70	1.14	1.25	0.38	–0.55	3.32
Mg#	55.36	54.75	54.67	56.10	57.86	55.26	55.17	57.76	56.23	60.20	66.29
Trace elements											
Nb	3	3	4	3	3		3	2	4	2	4
Zr	53	55	53	56	56		55	41	55	46	60
Y	25	24	22	23	24		25	20	24	20	26
Sr	73	72	70	71	69		70	67	71	82	360
Rb	4	3	3	3	2		1	2	2	1	4
Zn	96	101	101	98	94		99	87	96	86	80
Cu	190	201	202	196	201		199	176	196	150	115
Ni	78	76	76	76	78		75	83	74	98	252
Cr	48	50	46	43	52		46	52	46	238	678
V	377	371	380	362	385		388	405	378	304	302
Ba	46	95	43	39	44		42	35	44	51	168

Notes: Sample 163-989B-2R-1 (Piece 5, 83–88 cm) was crushed to sand size and cleaned using an ultrasonic probe. The suspended clay fraction was drawn off the overlying water column after resting 7 hr. The procedure was repeated until the water remained clear. Both the cleaned residue and clay fraction were analyzed. Sample 152-917A-101R-4, 81–85 cm, from Larsen, Saunders, Clift, et al. (1994). Fe_2O_3(t) = total iron as Fe_2O_3; LOI = loss on ignition; Mg# = 100[MgO/(MgO + FeO)] (molecular oxide amounts) with Fe_2O_3/FeO = 0.15. All determinations by X-ray-fluorescence spectrometry (analysts Don Sims and Joel Sparks). Sample 152-917A-101R-4, 81–85 cm, from Larsen, Saunders, Clift, et al. (1994).

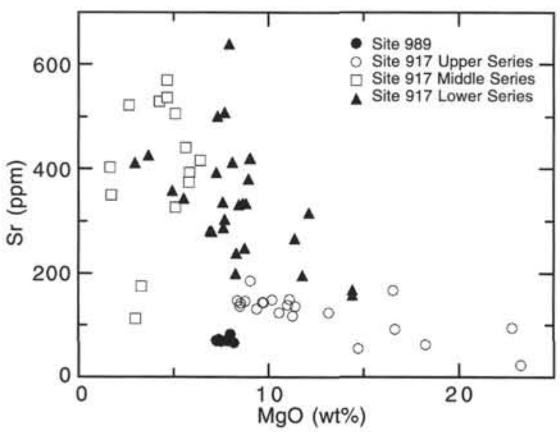

Figure 16. Sr vs. MgO for basalts from Site 989 compared with basalts from Site 917. Site 917 analyses are from Fitton et al. (in press).

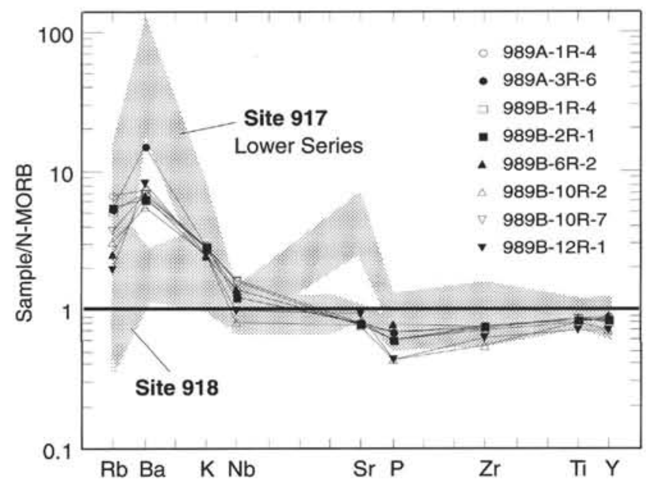

Figure 17. Spidergram of analyzed samples from Site 989 compared with basalts from the Site 917 Lower Series and Site 918, normalized to normal-MORB (Sun and McDonough, 1989). The fields for the basalts from Sites 917 and 918 are based on data from Fitton et al. (in press). The Site 917 data are from the Lower Series and include only samples with 6%–9% MgO; samples with high Nb/Zr were also excluded.

Ba and Sr spikes characteristic of the Site 917 Lower Series and attributed by Fitton et al. (in press) to assimilation of a Ba- and Sr-rich continental component. If the Site 989 lavas are contaminated, it is either to a much smaller degree or by a contaminant different from that in the Site 917 basalts.

Alteration

All rocks recovered from Site 989 contain low-temperature secondary phases that replace primary minerals and mesostasis and fill veins and vesicles. The distribution of secondary minerals was recorded in the alteration and vein logs for Holes 989A and 989B (on the back-pocket CD-ROM) and is shown in Figure 18.

The basalts of Unit 1 are moderately altered, with green smectitic clay completely replacing olivine and interstitial glass and lining or partly filling the abundant vesicles throughout the unit. Vesicles are open or partially or completely filled by smectite, zeolites, calcium

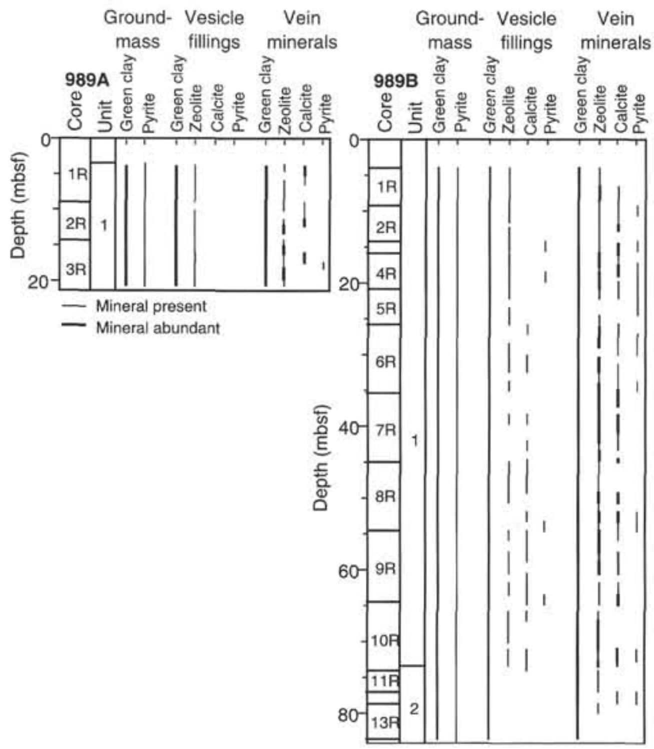

Figure 18. Distribution and abundance of secondary minerals at Site 989.

carbonate, and minor pyrite. Most vesicles have a thin lining of gray clay, although rare examples show that carbonate or zeolite is the earliest phase present. Zones of dominantly open or dominantly filled vesicles are present throughout the unit on about a 10-cm scale. Flow lobe boundaries are commonly the loci of more extensive alteration and contain large (~10 mm) zeolite-filled vesicles with 10-mm, very fine grained green halos. As Unit 1 becomes more massive, finer grained, and less vesicular toward its base, the majority of the vesicles are filled with green clay. Abundant vertical pipe vesicles at the base of Unit 1 are open or filled with calcite (Fig. 10).

Veins of secondary minerals are present throughout Unit 1. Green clay is the most abundant vein-filling material, although zeolite, calcium carbonate, and pyrite are common vein minerals, and many veins comprise a mixture of two or more of these phases. Most veins are lined with green clay, but examples of clay minerals postdating zeolite and/or carbonate were observed (e.g., clay-zeolite-pyrite vein in Section 163-989B-2R-1 [Piece 5, 93–95 cm]). Very rare veins have discontinuous pyrite linings. Coarse (1 cm) cleavage fragments of calcite are preserved on some broken vein surfaces in Cores 163-989B-8R and 9R (e.g., Section 163-989B-8R-4 [Piece 1C, 49 cm]). Distinct vein halos are not generally present, although large vesicles proximal (2–3 cm) to carbonate or zeolite veins are commonly completely filled with the vein mineral.

The complete alteration of the mesostasis and olivine of Unit 1 to massive brown clay is apparent in thin section. Areas of altered mesostasis commonly include minute (<1 μm) blebs of pyrite. Plagioclase, augite, and magnetite are generally unaltered, although the silicate phases can be partially altered to brown clays, particularly at grain margins and along cleavage planes. Concentric bands of two generations of greenish brown clay minerals line the rims of the vesicles, whereas the interior filling, where present, is either structureless or comprises an intergrowth of tiny (20 μm) circular clusters of radiating grains.

Unit 2 is a gray microcrystalline basalt with scattered vesicle segregation patches. The rock appears only slightly altered in hand specimen because of its fine grain size and low vesicularity. However, the unit is highly fractured, and the core is subdivided into 5–10-cm-sized fragments by thin (0.1–0.5 mm), randomly oriented veinlets filled with green clay and minor zeolite, calcium carbonate, and pyrite. Thin-section observation reveals the moderately altered nature of this unit, with the mesostasis and olivine completely replaced by brown clay minerals. The vesicles within the highly vesicular patches are filled with brown clay, and plagioclase and pyroxene are partially altered.

Secondary minerals were picked from veins and vesicles and identified by X-ray diffraction (XRD) (Table 8). A variety of zeolites is present, including stilbite, clinoptilolite, and heulandite. All samples of calcium carbonate that have been investigated by XRD are calcite. Green clays from vesicles and veins from both Holes 989A and 989B are randomly layered, saponite-dominated smectite/illite mixed-layer clays, except for Sample 163-989B-11R-1 (Piece 10, 89–90 cm), which has a more ordered mixed-layer structure.

The secondary mineral assemblages present at Site 989 are similar to those reported from subaerial flows in Iceland and the Faeroe Islands. However, the possibility of later, submarine alteration cannot be excluded. Detailed comparison with the alteration of lavas from nearby Site 917 must await shore-based analysis of the material from the sites.

Conclusions

Lava flows cored at Site 989 are interpreted from seismic data to lie stratigraphically below the lavas drilled at Site 917. Drilling at Site 989 was targeted to recover rocks from the oldest part of the SDRS along the EG63 transect.

Two lava flows were cored at Site 989. Unit 1 is at least 69 m thick, the thickest lava flow yet recorded from an SDRS (compare Roberts, Schnitker, et al., 1984; Eldholm, Thiede, Taylor, et al., 1987; Larsen, Saunders, Clift, et al., 1994). It is notable for its constant grain size, constant vesicularity, high mesostasis content, and repeated bands showing quench textures. These features indicate rapid cooling during solidification throughout the lava flow, which is difficult to reconcile with its great thickness. We interpret Unit 1 as a compound lava flow consisting of several lobes 0.1–10 m thick. The large number of thin flow lobes, together with the absence of sharp contacts between them, may indicate both (1) proximity to the eruptive vent and (2) rapid eruption of the entire lava flow. The observed decrease in maximum flow lobe thickness upward in the lava may reflect an exponentially diminishing eruption rate with time.

The basalts drilled at Site 989 are strongly depleted in a number of incompatible trace elements such as Zr, Nb, Ti, and P that suggest an origin in a depleted mantle source. The evolved composition of the basalts implies storage and fractionation of more primitive magmas before eruption. Storage may have occurred at either the crust/mantle boundary or within the continental crust that underlies this part of the volcanic succession (Larsen, Saunders, Clift, et al., 1994). Crustal magma chambers were invoked for the lavas in the Lower Series at Site 917 that have assimilated an Sr- and Ba-rich crustal component (Larsen, Saunders, Clift, et al., 1994). The incompatible element abundances (Fig. 17) suggest the possibility of crustal contamination of the Site 989 lavas, but the low Sr and Ba contents in these samples indicate either a smaller degree of contamination or a contaminant very different from that in the lavas at Site 917. Also, the possibility that alteration slightly increased Sr and Ba contents at the Site 989 lavas cannot be excluded without further study.

The two lava flows drilled at Site 989 differ in a number of ways from the lavas of the Lower Series at Site 917, and compositionally

Table 8. Secondary minerals from Site 989 identified by X-ray diffraction.

Core, section, piece, interval (cm)	Description	XRD identification
163-989A-		
3R-1 (Piece 1C, 83–83)	White platy zeolite with good cleavage	Stilbite
3R-3 (Piece 1A, 62–62)	Carbonate vein	Calcite
3R-4 (Piece 1A, 8–8)	Yellow mineral from zeolite-filled vesicle	Clinoptilolite
3R-4 (Piece 1C, 8–8)	Colorless euhedral mineral from same vesicle	Clinoptilolite
3R-4 (Piece 1A, 57–57)	Green clay vein (± pyrite)	Smectite/illite mixed-layer clay: random interlayers, mostly smectite
163-989B-		
6R-8 (Piece 3B, 79–80)	Glossy clay	Smectite/illite mixed-layer clay: random interlayers, mostly smectite; minor clinoptilolite and plagioclase
7R-1 (Piece 1B, 88–88)	Zeolite	Stilbite
7R-1 (Piece 2, 128–130)	Carbonate	Calcite
8R-4 (Piece 1C, 49–49)	Cleavage fragments of carbonate	Calcite (minor stilbite)
8R-6 (Piece 1B, 68–70)	Creamy carbonate from large vesicle (15 mm)	Calcite
8R-6 (Piece 1C, 108–109)	White zeolite	Stilbite
10R-6 (Piece 2B, 78–80)	Coarse carbonate	Calcite
10R-7 (Piece 2, 22–25)	Zeolite	Heulandite
10R-7 (Piece 6, 90–92)	Carbonate from tube vesicles	Calcite
11R-1 (Piece 10, 89–90)	Waxy green clay	Smectite/illite mixed-layer clay: ordered structure, mostly smectite; minor plagioclase
13R-2 (Piece 6, 28–32)	Waxy green clay	Smectite/illite mixed-layer clay: mostly smectite

they do not constitute a downward continuation of that series. In fact, they show greater similarities to the oceanic succession at Site 918 than to the continental succession at Site 917.

PHYSICAL PROPERTIES

Two holes were cored at Site 989. Hole 989A penetrated 20.2 m of igneous Unit 1, and Hole 989B penetrated 73.9 m of the same igneous Unit 1 and 8.2 m of the underlying igneous Unit 2 (see "Igneous Petrology" section, this chapter). The excellent recovery of basalt from this site allowed dense sampling of physical properties measurements, facilitating statistical correlations between the physical properties and other observations (e.g., petrology).

At Holes 989A and 989B, the measurement of *P*-wave velocities on split core sections was performed using the Hamilton Frame velocimeter; *P*-wave velocities and index properties were also measured on discrete minicore samples. In addition, magnetic susceptibility measurements were conducted on all split core sections using the MST. Thermal conductivity measurements were made on selected pieces from Hole 989B.

Acoustic Velocity

P-wave velocities were measured directly on seawater-saturated split core sections using the Hamilton Frame velocimeter. The velocity data are listed in Table 9 on the CD-ROM in the back pocket of this volume and plotted in Figure 19. In addition, the Hamilton Frame velocimeter was used to measure the *P*-wave velocities of discrete seawater-saturated samples (minicores). Discrete-sample positions were selected on the basis of a semiuniform sampling interval of approximately 1 minicore per 3 m throughout both holes.

The split-core velocity measurements for the upper 20 m of Hole 989B correlate well with the measurements from Hole 989A. This is expected, because Hole 989B is located less than 3 m from Hole 989A (see "Operations" section, this chapter). The good correlation between the holes gives credence to the ability of the Hamilton Frame split-core velocity measurement technique to provide reliable results. In light of this conclusion, a large amount of time and effort was given to acquiring extensive sets of split-core velocity measurements. The average *P*-wave velocities on the split core sections are as follows: Hole 989A Unit 1, 4.98 ± 0.15 km/s; Hole 989B Unit 1, 4.97 ± 0.15 km/s; and Hole 989B Unit 2, 6.03 ± 0.20 km/s. The relatively small standard deviations of the velocity measurements reveal the generally homogeneous character within each of the igneous units.

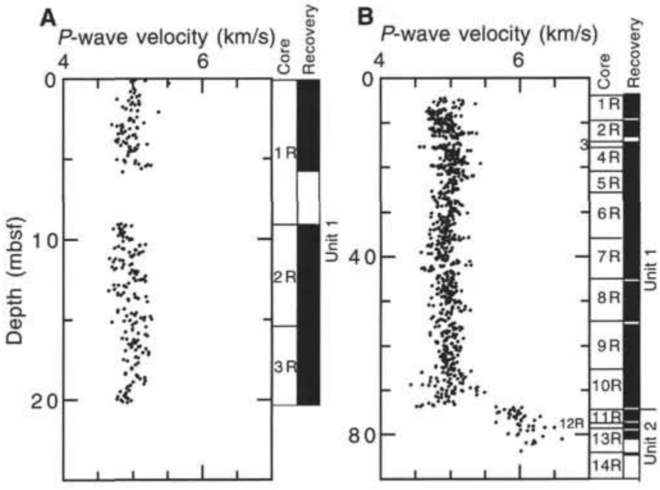

Figure 19. Downcore profile of *P*-wave velocity measurements performed directly on seawater-saturated split core sections from (**A**) Hole 989A and (**B**) Hole 989B. Note the high percentage of core recovery and the abrupt velocity change between Units 1 and 2 in Hole 989B. The measurement error is 0.03 km/s.

However, a spectral analysis of the velocity data from Hole 989B Unit 1 (Fig. 20) displays a subtle variation within the seismic data with a dominant peak in the frequency spectrum corresponding to a characteristic wavelength of ~5.6 m. A comparison of this feature with those described in the "Igneous Petrology" section (this chapter) appears to correlate with the longer wavelength (~6 m) basaltic flow lobes within compound flow Unit 1 (Fig. 12). These velocity variations appear to be related to porosity changes within the flows.

The *P*-wave velocities measured on seawater-saturated minicores were performed in the same manner as the split-core measurements (see above) and are listed in Table 10. The average minicore *P*-wave velocities are as follows: Hole 989A Unit 1, 5.13 ± 0.16 km/s; Hole 989B Unit 1, 5.19 ± 0.24 km/s; and Hole 989B Unit 2, 6.17 ± 0.18 km/s. Thus, there is a 3% average difference between split-core and minicore velocity measurements. This difference may be due to drilling-induced cracks on the outer walls of the split core sections that are not present on the sampled, cylindrical minicores. The effect of these cracks is to lower the effective modulus and, in turn, reduce the seismic velocity. Additionally, note that all velocity measurements

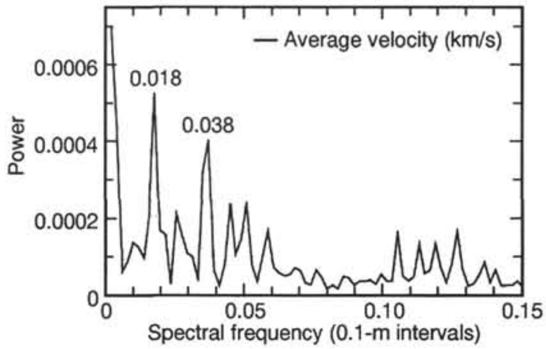

Figure 20. Spectral analysis plot of velocity data from Hole 989B Unit 1 averaged over 0.1-m intervals. The dominant frequency corresponds to a wavelength of ~5.6 m, which correlates well with the longer wavelength (~6 m) basaltic flows within igneous Unit 1, as discussed in the "Igneous Petrology" section (this chapter).

were taken at atmospheric pressure and must be extrapolated to in situ pressure regimes for correlation with the integrated traveltimes obtained from seismic surveys.

Index Properties

Index properties measurements (bulk density, grain density, porosity, and percent water content) were performed on discrete samples (minicores) from Holes 989A and 989B. These data are listed in Table 10.

The average grain densities of 2.91 ± 0.06 g/cm^3, 2.89 ± 0.08 g/cm^3, and 2.95 ± 0.01 g/cm^3 for Hole 989A Unit 1 and Hole 989B Units 1 and 2, respectively, are slightly less than the average grain density for basalt, 3.01 ± 0.14 g/cm^3 (Johnson and Olhoeft, 1984), but fall within 1 standard deviation of the mean. This seems to indicate that the dominant particle lithology is quite consistent with that of basalt. The slight discrepancy may be due to the presence of less dense clays (e.g., smectite average grain density ~2.67 g/cm^3) filling many of the vesicles within the basaltic samples (see "Igneous Petrology" section, this chapter).

The calculated percent water content and porosity are also quite consistent within each unit. Average porosities of more than 10% are present within the Unit 1 samples from Holes 989A and 989B, whereas the finer grained Unit 2 samples of Hole 989B reveal a significant decrease in porosity to an average value of less than 2.5%. The linear correlation coefficient between *P*-wave modulus and porosity is 0.74 for the suite of minicores measured from Site 989 (Fig. 21).

Magnetic Susceptibility

As a result of the necessary hardware and software upgrades performed on the MST during Leg 163, the only operational instrument of the MST during the drilling at Site 989 was the magnetic susceptibility meter. This instrument came on line shortly after the initiation of the drilling of Hole 989A. Because some of the cores had already been longitudinally split, magnetic susceptibility measurements were performed on the split core sections; however, the susceptibility meter was calibrated for whole cores only. With that in mind, volume correction factors must be applied when analyzing the data set. The complete data set is given in Table 11 on the CD-ROM in the back pocket of this volume, and a plot of magnetic susceptibility vs. depth is shown in Figure 22. Magnetic susceptibility values range from 730×10^{-5} to 1500×10^{-5} SI for Unit 1 and from 500×10^{-5} to 1000×10^{-5} SI for Unit 2. The break between Units 1 and 2 at a depth of 73.9 mbsf can be clearly seen in the plot. Also, the higher susceptibility measurements at the base of Unit 1 appear to correlate with the location of a single thick (>10 m) flow lobe as indicated in the "Igneous Petrology" section, this chapter (Table 6; Fig. 12).

Thermal Conductivity

Thermal conductivity was measured on three samples from Site 989. In addition, an experiment was undertaken to test the statistical reliability of the thermal conductivity measurement techniques. To maintain constant temperature, samples were measured in a water bath under a small overburden pressure. This also created a better contact between the sample and the half-space line source. Measurements were conducted on both unpolished and polished pieces. The results are listed in Table 12. The data reveal smaller standard deviations for the measurements performed on polished, compared with unpolished, pieces. This can be attributed to the enhanced contact between the line source and the samples with polished surfaces. Thus, when possible, samples should be polished before measuring thermal conductivity. Also, the relatively large standard deviations of the measurements (6%–8%) indicate that multiple measurements on individual samples need to be performed to acquire statistically meaningful results. The average thermal conductivity value for the three measured polished samples is 1.82 ± 0.20 $Wm^{-1}K^{-1}$. This value is consistent with the average values listed for basalt from Hole 917A (i.e., 1.73 ± 0.25 $Wm^{-1}K^{-1}$; Larsen, Saunders, Clift, et al., 1994).

Summary

The physical properties results from Site 989 clearly reveal two distinct units, igneous Unit 1 and igneous Unit 2. The contrast in physical properties between the two units correlates well with changes in texture and vesicularity (see "Igneous Petrology" section, this chapter).

The coarser grained, highly vesicular, aphyric basalt of Unit 1 possesses lower elastic moduli and bulk densities, higher porosity and water contents, and higher magnetic susceptibility values than the underlying, finer grained, plagioclase-phyric basalt of Unit 2.

Dense sampling of *P*-wave velocities was performed directly on seawater-saturated split core sections throughout the recovered units. This unique data set reveals interesting small-scale velocity variations that correlate well with petrologic observations. The elastic moduli, and hence seismic velocities, of the samples are correlatable in the following manner: the higher the porosity, the lower the elastic modulus (or similarly, the seismic velocity). Thus, if porosity or vesicularity can reveal the cooling history of flow units and porosity in turn relates to seismic velocity, detailed seismic velocity profiles may help in imaging and understanding the formation and cooling history of compound basaltic flows.

REFERENCES

Berggren, W.A., Kent, D.V., Swisher, C.C., III, and Aubry, M.-P., 1995. A revised Paleogene geochronology and chronostratigraphy. *In* Berggren, W.A., Kent, D.V., and Hardenbol, J. (Eds.), *Geochronology, Time Scales and Stratigraphic Correlation: Framework for an Historical Geology.* Spec. Publ.—Soc. Econ. Paleontol. Mineral., 54:129–212.

Eldholm, O., Thiede, J., Taylor, E., et al., 1987. *Proc. ODP, Init. Repts.,* 104: College Station, TX (Ocean Drilling Program).

Fitton, J.G., Saunders, A.D., Larsen, L.M., Hardarson, B.S., and Norry, M.J., in press. Volcanic rocks from the East Greenland Margin at 63°N: composition, petrogenesis, and mantle sources. *In* Saunders, A.D., Larsen, H.C., Clift, P.D., and Wise, S.W., Jr. (Eds.), *Proc. ODP, Sci. Results,* 152: College Station, TX (Ocean Drilling Program).

Johnson, G.R., and Olhoeft, G.R., 1984. Density of rocks and minerals. *In* Carmichael, R.S. (Ed.), *CRC Handbook of Physical Properties of Rocks* (Vol. 3): Boca Raton, FL (CRC Press), 1–38.

Larsen, H.C., and Jakobsdóttir, S., 1988. Distribution, crustal properties and significance of seaward-dipping sub-basement reflectors off East Greenland. *In* Morton, A.C., and Parson, L.M. (Eds.), *Early Tertiary Volcanism* *and the Opening of the Northeast Atlantic:* Geol. Soc. Spec. Publ. London, 39:95–114.

Larsen, H.C., Saunders, A.D., Clift, P.D., et al., 1994. *Proc. ODP, Init. Repts.,* 152: College Station, TX (Ocean Drilling Program).

Merrill, R.T., and McElhinny, M.W., 1983. *The Earth's Magnetic Field: Its History, Origin, and Planetary Perspective:* London (Acad. Press).

Roberts, D.G., Schnitker, D., et al., 1984. *Init. Repts. DSDP,* 81: Washington (U.S. Govt. Printing Office).

Sinton, C.W., and Duncan, R.A., in press. $^{40}Ar/^{39}Ar$ ages of lavas from the southeast Greenland margin, ODP Leg 152, and the Rockall Plateau, DSDP Leg 81. *In* Saunders, A.D., Larsen, H.C., Clift, P.D., and Wise, S.W., Jr. (Eds.), *Proc. ODP, Sci. Results,* 152: College Station, TX (Ocean Drilling Program).

Sinton, C.W., Larsen, H.C., and Duncan, R.A., 1994. The timing of the volcanism at the southeast Greenland Margin, ODP Leg 152. *Eos,* 75:607.

Soper, N.J., Higgins, A.G., Downie, C., Matthews, D.W., and Brown, P.E., 1976. Late Cretaceous–early Tertiary stratigraphy of the Kangerdlugssuaq area, east Greenland, and the age of opening of the north-east Atlantic. *J. Geol. Soc. London,* 132:85–104.

Sun, S.-S., and McDonough, W.F., 1989. Chemical and isotopic systematics of oceanic basalts: implications for mantle composition and processes. *In* Saunders, A.D., and Norry, M.J. (Eds.), *Magmatism in the Ocean Basins.* Geol. Soc. Spec. Publ. London, 42:313–345.

Ms 163IR-104

NOTE: For all sites drilled, core-description forms ("barrel sheets") and core photographs can be found in Section 3, beginning on page 71. Thin-section data can be found in Section 4, beginning on page 253. See Table of Contents for material contained on CD-ROM.

Table 10. *P*-wave velocity and index properties measured on discrete, 1-in.-diameter minicores from Holes 989A and 989B.

		Saturated			Dry						
Core, section, interval (cm)	Depth (mbsf)	*P*-wave velocity (km/s)	Mass (g)	Volume (cm^3)	Mass (g)	Volume (cm^3)	Bulk density (g/cm^3)	Water content (%)	Porosity (%)	Grain density (g/cm^3)	Comments
Unit 1											
163-989A-											
1R-1, 127–129	1.27	5.15	33.056	12.12	31.232	10.50	2.73	5.70	15.0	2.98	Nonvesicular
1R-3, 36–38	2.82	5.02	28.442	10.09	27.339	9.31	2.82	4.01	10.7	2.94	Small vesicles
1R-3, 56–58	3.02	5.29	29.537	10.49	28.189	9.61	2.82	4.72	12.4	2.94	Large vesicles
2R-2, 97–99	11.08	5.21	30.577	10.86	29.356	10.10	2.82	4.12	10.9	2.91	Crack
2R-4, 91–93	13.17	5.07	32.543	11.77	30.938	10.77	2.76	5.10	13.1	2.87	"Average" sample
2R-5, 23–25	13.5	5.32	30.673	10.92	29.510	10.59	2.81	3.92	10.0	2.79	Large vesicles
3R-1, 2–4	14.32	5.28	31.832	11.52	30.618	10.79	2.76	3.94	10.2	2.84	Medium grained, small amount of vesicles
3R-3, 77–79	16.91	5.02	29.522	10.67	28.125	9.45	2.77	4.89	13.0	2.98	Vesicular
3R-6, 16–18	19.94	4.83	34.908	12.45	33.211	11.42	2.80	5.02	13.1	2.91	
Mean		5.13					2.79	4.60	12.1	2.91	
Standard deviation		0.16					0.03	0.63	1.7	0.06	
163-989B-											
1R-2, 44–46	5.83	5.53	36.817	13.25	35.461	12.49	2.78	3.81	9.9	2.84	Small vesicles, crack
1R-3, 51–53	7.12	5.00	35.494	12.79	34.162	11.82	2.78	3.88	10.2	2.89	
1R-4, 91–93	8.85	4.88	30.647	11.02	29.416	10.17	2.78	4.15	10.9	2.89	Zeolite-filled vein
2R-1, 21–23	9.41	4.93	29.497	10.72	28.306	10.18	2.75	4.17	10.6	2.78	Small vesicles
2R-2, 60–62	11.04	5.04	28.542	10.37	27.172	9.64	2.75	4.96	12.6	2.82	Vesicular
2R-3, 40–42	12.08	5.33	30.940	11.06	29.717	10.42	2.80	4.08	10.6	2.85	
3R-1, 28–30	14.48	5.15	31.843	11.33	30.681	10.54	2.81	3.77	10.0	2.91	Small vesicles
3R-1, 120–122	15.40	4.89	28.088	10.30	26.716	9.45	2.73	5.05	12.8	2.83	Large vesicles
4R-1, 136–138	17.26	5.20	32.168	11.61	30.789	10.76	2.77	4.43	11.5	2.86	Large vesicles
4R-3, 43–45	19.05	5.42	35.194	12.36	34.302	12.02	2.85	2.62	7.0	2.85	Vesicular
4R-4, 6–8	19.98	5.05	29.775	10.59	28.622	10.01	2.81	4.00	10.4	2.86	Medium vesicles
5R-1, 22–24	21.02	5.21	30.659	10.84	29.546	10.40	2.83	3.75	9.8	2.84	Vesicular
5R-2, 137–139	23.56	5.15	32.595	11.75	31.204	11.03	2.77	4.41	11.3	2.83	Vesicular
5R-4, 26–28	24.73	5.26	28.984	10.70	27.246	9.31	2.71	6.20	15.9	2.93	Zeolite-filled vein
6R-1, 124–126	27.04	5.09	28.502	10.33	27.071	9.59	2.76	5.19	13.1	2.83	
6R-7, 129–131	35.15	5.20	28.513	10.18	27.378	9.47	2.80	4.11	10.8	2.89	Medium grained, small vesicles
7R-1, 109–111	36.59	6.01	30.091	10.60	28.968	9.78	2.84	3.86	10.4	2.97	Medium grained, small vesicles
7R-3, 79–81	39.23	5.22	30.579	10.93	29.371	10.24	2.80	4.08	10.7	2.87	Fine grained
8R-2, 28–30	46.86	5.19	31.571	11.35	30.109	10.44	2.78	4.78	12.4	2.89	Filled vesicles
8R-6, 50–52	52.30	5.03	32.941	11.89	31.251	10.15	2.77	5.30	14.4	3.08	Small amount of large vesicles
9R-1, 129–131	55.99	5.20	33.653	11.98	32.313	10.61	2.81	4.11	11.3	3.05	Vesicular
9R-3, 8–10	57.61	4.97	31.171	11.16	29.746	10.19	2.79	4.72	12.4	2.92	Medium grained, vesicular
9R-8, 5–7	64.76	5.12	35.964	12.86	34.595	12.06	2.80	3.93	10.3	2.87	Medium grained, filled vesicles
10R-3, 60–62	67.89	5.49	32.028	11.45	30.709	10.00	2.80	4.25	11.8	3.07	Fine grained, filled vesicles
10R-4, 8–10	68.78	5.31	32.635	11.75	31.003	10.71	2.78	5.17	13.4	2.90	Medium grained
Mean		5.19					2.79	4.35	11.4	2.89	
Standard deviation		0.24					0.03	0.71	1.8	0.08	
Unit 2											
163-989B-											
11R-1, 134–136	75.44	6.00	37.784	12.56	37.485	12.72	3.01	0.82	2.3	2.95	Fine grained, nonvesicular
12R-1, 88–90	77.98	6.15	33.510	11.17	33.235	11.30	3.00	0.82	2.4	2.94	Fine grained, nonvesicular
13R-2, 106–108	81.16	6.36	39.246	13.06			3.01				Fine grained, nonvesicular
Mean		6.17					3.01	0.83	2.4	2.95	
Standard deviation		0.18					0.01	0.02	0.1	0.00	

Notes: Salinity = 0.032; pore-fluid density = 1.022 g/cm^3. The relatively small standard deviations of the mean for each set of measurements indicate subtle variations within each unit. Also, the coarser grained, aphyric basalts of Unit 1 have much greater porosities and lower *P*-wave velocities than the underlying plagioclase-phyric basalts of Unit 2.

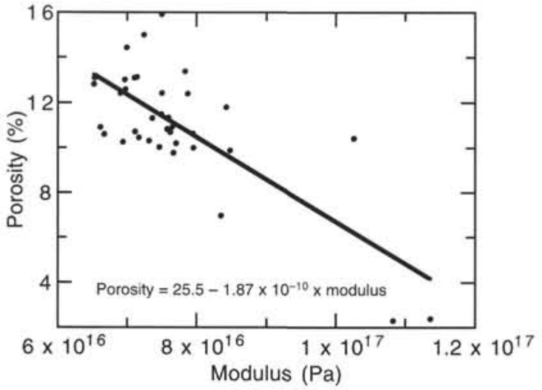

Figure 21. Plot of *P*-wave modulus as a function of porosity for all minicores sampled from Holes 989A and 989B. Variation in the pore aspect ratios may be responsible for much of the scatter in the data, but a relatively good linear correlation (R = 0.74) exists for this simple relationship.

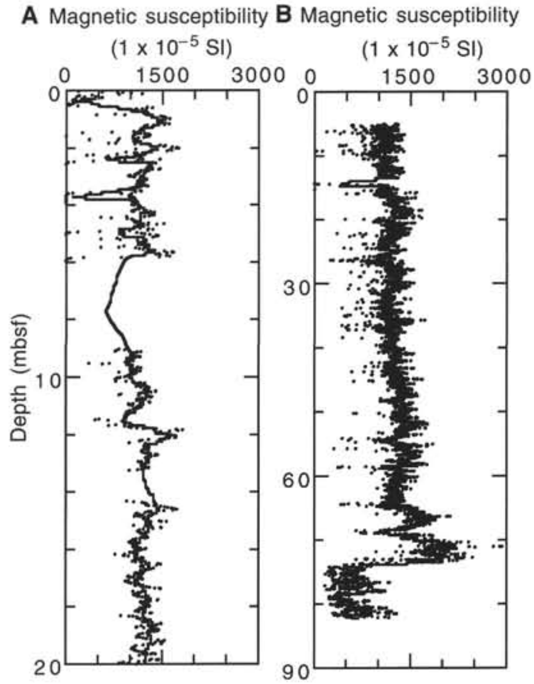

Figure 22. Magnetic susceptibility vs. depth for the recovered interval from (**A**) Hole 989A and (**B**) Hole 989B. Magnetic susceptibility was measured directly on split core sections using the MST. The dots represent raw data, and the line represents a 15-point running average.

Table 12. Tabulated results of a thermal conductivity ($Wm^{-1}K^{-1}$) experiment designed to deduce the reliability of measurement techniques.

	163-989B-1R-2		162-989B-8R-5		162-989B-10R-3	
	Unpolished	Polished	Unpolished	Polished	Unpolished	Polished
	1.71	1.44	1.63	1.98	2.13	1.88
	1.64	1.67	1.77	1.85	1.89	1.89
	2.28	1.63	1.52	1.78	2.12	2.15
	1.70		1.35			1.89
Average	1.83	1.58	1.57	1.87	2.04	1.95
Standard deviation	0.30	0.12	0.18	0.10	0.14	0.13

Notes: Measurements were made on both unpolished individual pieces after the cores were split using the circular saw and on polished samples. Polishing the samples enhanced thermal coupling with the half-space line source (Needle 326), producing more statistically meaningful results.